Available online at www.sciencedirect.com
ScienceDirect
International Journal of Heat and Mass Transfer 50 (2007) 766–775
International Journal of HEAT and MASS TRANSFER
www.elsevier.com/locate/ijhmt

Steady natural convection flows in a square cavity with linearly heated side wall(s)

M. Sathiyamoorthy [a], Tanmay Basak [b], S. Roy [c], I. Pop [d,*]

[a] Department of Applied Mathematics, Birla Institute of Technology, Mesra, Ranchi 835215, India
[b] Department of Chemical Engineering, Indian Institute of Technology Madras, Chennai 600036, India
[c] Department of Mathematics, Indian Institute of Technology Madras, Chennai 600036, India
[d] Faculty of Mathematics, University of Cluj, R-3400 Cluj, CP 253, Romania

Received 30 January 2006
Available online 13 November 2006

Abstract

The present numerical study deals with natural convection flow in a closed square cavity when the bottom wall is uniformly heated and vertical wall(s) are linearly heated whereas the top wall is well insulated. Non-linear coupled PDEs governing the flow have been solved by penalty finite element method with bi-quadratic rectangular elements. Numerical results are obtained for various values of Rayleigh number (Ra) ($10^3 \leqslant Ra \leqslant 10^5$) and Prandtl number ($Pr$) ($0.7 \leqslant Pr \leqslant 10$). Results are presented in the form of streamlines, isotherm contours, local Nusselt number and the average Nusselt as a function of Rayleigh number.

Keywords: Penalty finite element method; Natural convection; Square cavity; Non-uniform heating

1. Introduction

The phenomenon of natural convection in enclosures has received considerable attention in recent years. This attention is due to mainly because this phenomenon often affects the thermal performance in many engineering and science applications such as boilers, nuclear reactor systems, energy storage and conservation, fire control and chemical, food and metallurgical industries.

Buoyancy driven flows are complex because of essential coupling between the transport properties of flow and thermal fields. In particular, internal flow problems are considerably more complex than external ones. This is because at large Rayleigh number (product of Prandtl and Grashof numbers) classical boundary layer theory yields the simplifications for external flow problems, namely, the region exterior to the boundary layer is unaffected by the boundary layer. For confined natural convection, in contrast, boundary layers form near the walls but the region exterior to them in enclosed by the boundary layers form a core region. Since the core is partially or fully encircled by the boundary layers, the core flow is not readily determined from the boundary conditions but depend on the boundary layer, which, in turn is influenced by the core. The interactions between the boundary layer and core constitute a major complexity in the problem. In fact, the situation is even more intricate because it often appears that more than one global core flow is possible and flow sub-regions, such as, cells and layers, may be embedded in the core. A literature survey shows that the comprehensive review of these problems was made by Ostrach [1–3], Gebhart [4] and Hoogendoorn [5] in which each emphasizes essentially various aspects of the subject.

Among the earlier studies, it may be noted that Fusegi et al. [6], Lage and Bejan [7,8], and Xia and Murthy [9] have made attempts to acquire a basic understanding of natural convection flows and transfer characteristics in an enclosure where one vertical wall is cooled and another

* Corresponding author. Tel.: +40 264 594315; fax: +40 264 591906.
E-mail addresses: tanmay@iitm.ac.in (T. Basak), sjroy@iitm.ac.in (S. Roy), pop.ioan@yahoo.co.uk (I. Pop).

0017-9310/$ - see front matter © 2006 Published by Elsevier Ltd.
doi:10.1016/j.ijheatmasstransfer.2006.06.019

Nomenclature

g	acceleration due to gravity, m s^{-2}
k	thermal conductivity, W m^{-1} K^{-1}
L	side of the square cavity, m
n	the normal direction on a cavity wall
N	total number of nodes
Nu	local Nusselt number
Nu_b	local Nusselt number at the bottom wall
Nu_l	local Nusselt number at the left wall
Nu_r	local Nusselt number at the right wall
Nu_s	local Nusselt number at the side wall
$\overline{Nu}_b$	average Nusselt number at the bottom wall
$\overline{Nu}_s$	average Nusselt number at the side wall
p	pressure, Pa
P	dimensionless fluid pressure
Pr	Prandtl number
Ra	Rayleigh number
T	fluid temperature, K
T_c	temperature of cold (right) wall, K
T_h	temperature of hot (bottom) wall, K
u	x component of velocity
U	x component of dimensionless velocity
v	y component of velocity
V	y component of dimensionless velocity
X	dimensionless distance along x-coordinate
Y	dimensionless distance along y-coordinate

Greek symbols

α	thermal diffusivity, m^2 s^{-1}
β	volume expansion coefficient, K^{-1}
γ	penalty parameter
θ	dimensionless temperature
ν	kinematic viscosity, m^2 s^{-1}
ρ	density, kg m^{-3}
ψ	stream function

Subscripts

b	bottom wall
c	cooled wall
h	hot wall
l	left wall
r	right wall
s	side wall

one heated while the remaining top and bottom walls are well insulated. November and Nansteel [10] and Valencia and Frederick [11] have shown a specific interest to focus on a natural convection within a rectangular enclosure wherein a bottom heating and/or a top cooling are involved. Studies on natural convection in a rectangular enclosures heated from below and cooled along a single side or both sides have been carried out by Ganzarolli and Milanez [12]. Recently, Corcione [13] has studied a natural convection in a air-filled rectangular enclosure heated from below and cooled from above for a variety of thermal boundary conditions at the side walls. Numerical results were reported for several values of both width-to-height aspect ratio of enclosure and Rayleigh number. Further, Sarris et al. [14] have also reported recently the effect of sinusoidal top wall temperature variations in a natural convection within a square enclosure where the other walls are insulated.

The aim of the present paper is to study the circulations, temperature distributions within a square cavity and heat transfer rate at the heated walls in terms of local and average Nusselt numbers as a function Rayleigh number when the bottom wall is heated uniformly, left vertical wall is heated linearly and right vertical wall is either linearly heated or cooled. In any case, the top wall is well insulated. In the case of cooled vertical wall, the finite discontinuity in temperature distribution appear at the right edge of the bottom wall. In the current study, Galerkin finite element method with penalty parameter has been used to solve the non-linear coupled partial differential equations for flow and temperature field.

2. Mathematical formulation

Thermophysical properties of the fluid in the flow model assumed to be constant except the density variations causing a body force term in the momentum equation. The Boussinesq approximation is invoked for the fluid properties to relate density changes to temperature changes, and to couple in this way the temperature field to the flow field. The governing equations for the steady natural convection flow using conservation of mass, momentum and energy can be written as

$$\frac{\partial u}{\partial x}+\frac{\partial v}{\partial y}=0, \tag{1}$$

$$u\frac{\partial u}{\partial x}+v\frac{\partial u}{\partial y}=-\frac{1}{\rho}\frac{\partial p}{\partial x}+\nu\left(\frac{\partial^2 u}{\partial x^2}+\frac{\partial^2 u}{\partial y^2}\right), \tag{2}$$

$$u\frac{\partial v}{\partial x}+v\frac{\partial v}{\partial y}=-\frac{1}{\rho}\frac{\partial p}{\partial y}+\nu\left(\frac{\partial^2 v}{\partial x^2}+\frac{\partial^2 v}{\partial y^2}\right)+g\beta(T-T_c), \tag{3}$$

$$u\frac{\partial T}{\partial x}+v\frac{\partial T}{\partial y}=\alpha\left(\frac{\partial^2 T}{\partial x^2}+\frac{\partial^2 T}{\partial y^2}\right) \tag{4}$$

with boundary conditions

$$u(x,0)=u(x,L)=u(0,y)=u(L,y)=0,$$
$$v(x,0)=v(x,L)=v(0,y)=v(L,y)=0,$$
$$T(x,0)=T_h,\quad \frac{\partial T}{\partial y}(x,L)=0,\quad 0<x<L,$$
$$T(0,y)=T_h-(T_h-T_c)\frac{y}{L},$$
$$T(L,y)=T_h-(T_h-T_c)\frac{y}{L}\quad\text{or}\quad T_c \tag{5}$$

here x and y are the distances measured along the horizontal and vertical directions, respectively; u and v are the velocity components in the x- and y-directions, respectively, T denotes the temperature; p is the pressure and ρ is the density; T_h and T_c are the temperature at hot and cold walls, respectively; L is the side of the square of cavity.

Using the following change of variables:

$$X=\frac{x}{L},\quad Y=\frac{y}{L},\quad U=\frac{uL}{\alpha},\quad V=\frac{vL}{\alpha},\quad \theta=\frac{T-T_c}{T_h-T_c},$$
$$P=\frac{pL^2}{\rho\alpha^2},\quad Pr=\frac{\nu}{\alpha},\quad Ra=\frac{g\beta(T_h-T_c)L^3Pr}{\nu^2}. \tag{6}$$

The governing equations (1)–(4) reduce to non-dimensional form as

$$\frac{\partial U}{\partial X}+\frac{\partial V}{\partial Y}=0, \tag{7}$$
$$U\frac{\partial U}{\partial X}+V\frac{\partial U}{\partial Y}=-\frac{\partial P}{\partial X}+Pr\left(\frac{\partial^2 U}{\partial X^2}+\frac{\partial^2 U}{\partial Y^2}\right), \tag{8}$$
$$U\frac{\partial V}{\partial X}+V\frac{\partial V}{\partial Y}=-\frac{\partial P}{\partial Y}+Pr\left(\frac{\partial^2 V}{\partial X^2}+\frac{\partial^2 V}{\partial Y^2}\right)+Ra\,Pr\theta, \tag{9}$$
$$U\frac{\partial \theta}{\partial X}+V\frac{\partial \theta}{\partial Y}=\left(\frac{\partial^2 \theta}{\partial X^2}+\frac{\partial^2 \theta}{\partial Y^2}\right) \tag{10}$$

with the boundary conditions

$$U(X,0)=U(X,1)=U(0,Y)=U(1,Y)=0,$$
$$V(X,0)=V(X,1)=V(0,Y)=V(1,Y)=0,$$
$$\theta(X,0)=1,\quad \frac{\partial\theta}{\partial Y}(X,1)=0,$$
$$\theta(0,Y)=1-Y,\quad \theta(1,Y)=1-Y\quad \text{or } \theta(1,Y)=0. \tag{11}$$

Here X and Y are dimensionless coordinates varying along horizontal and vertical directions, respectively; U and V are dimensionless velocity components in the X- and Y-directions, respectively; θ is the dimensionless temperature; P is dimensionless pressure; Ra and Pr are Rayleigh and Prandtl numbers, respectively.

3. Numerical method and choice of parameters

The momentum and energy balance equations (8)–(10) are solved using the Galerkin finite element method. The continuity equation (7) will be used as a constraint due to mass conservation and this constraint may be used to obtain the pressure distribution [15,16]. In order to solve Eqs. (8)–(10), we use the penalty finite element method where the pressure P is eliminated by a penalty parameter γ and the incompressibility criteria by Eq. (7) (see Reddy [15]) which results in

$$P=-\gamma\left(\frac{\partial U}{\partial X}+\frac{\partial V}{\partial Y}\right). \tag{12}$$

The continuity equation (7) is automatically satisfied for large value of γ. Typical values of γ that yield consistent solutions are 10^7 [15,16].

Using Eq. (12), the momentum balance equations (8) and (9) reduce to

$$U\frac{\partial U}{\partial X}+V\frac{\partial U}{\partial Y}=\gamma\frac{\partial}{\partial X}\left(\frac{\partial U}{\partial X}+\frac{\partial V}{\partial Y}\right)+Pr\left(\frac{\partial^2 U}{\partial X^2}+\frac{\partial^2 U}{\partial Y^2}\right) \tag{13}$$

and

$$U\frac{\partial V}{\partial X}+V\frac{\partial V}{\partial Y}=\gamma\frac{\partial}{\partial Y}\left(\frac{\partial U}{\partial X}+\frac{\partial V}{\partial Y}\right)+Pr\left(\frac{\partial^2 V}{\partial X^2}+\frac{\partial^2 V}{\partial Y^2}\right)+Ra\,Pr\theta. \tag{14}$$

The system of Eqs. (10), (13) and (14) with the boundary conditions (11) is solved using Galerkin finite element method. Since the solution procedure is explained in Ref. [16], the detailed description is not included in this paper. The numerical solutions are obtained in terms of velocity components (U, V) and the stream function (ψ) is evaluated using the relationship between the stream function (ψ) and velocity components [17]. It may be noted that the positive sign of ψ denotes anti-clockwise circulation and the clockwise circulation is represented by the negative sign of ψ. The no-slip condition is valid at all boundaries as there is no cross-flow, hence $\psi=0$ is used for the boundaries.

The heat transfer coefficient in terms of the local Nusselt number is defined by

$$Nu=\frac{-\partial\theta}{\partial n}, \tag{15}$$

where n-denotes the normal direction on a plane. The local Nusselt number at bottom wall (Nu_b) and at the side wall (Nu_s) are evaluated for various wall boundary conditions using the above definition. The average Nusselt numbers at the bottom and side walls are computed as follows:

$$\overline{Nu_b}=\int_0^1 Nu_b\,dX\quad\text{and}\quad \overline{Nu_s}=\int_0^1 Nu_s\,dY. \tag{16}$$

The computational domain consists of 20×20 bi-quadratic elements which correspond to 41×41 grid points. The bi-quadratic elements smoothly capture the non-linear variations of the field variables which are in contrast with finite difference/finite volume solutions available in the literature [4,5]. In order to assess the accuracy of the numerical procedure, the present algorithm based on the grid size (41×41) for a square enclosure have been tested with the work of Mallinson and Vahl Davis [18] for $Ra=10^3$–10^5. Computations have been carried out for various values of $Ra=10^3$–10^5 and $Pr=0.7$–10 with uniformly heated bottom wall, linearly heated left wall and linearly heated or cooled right wall where the top wall is well insulated as described in Section 4. Further, computations for $Pr=0.01$, 0.1, 0.3 and 0.5 as well as $Pr=1$, 100 and 1000 have also been done but the results are not described here as no specific different features have been observed. In case of cooled right wall, the jump discontinuity of Dirichlet type boundary condition at the corner point (see Fig. 1)

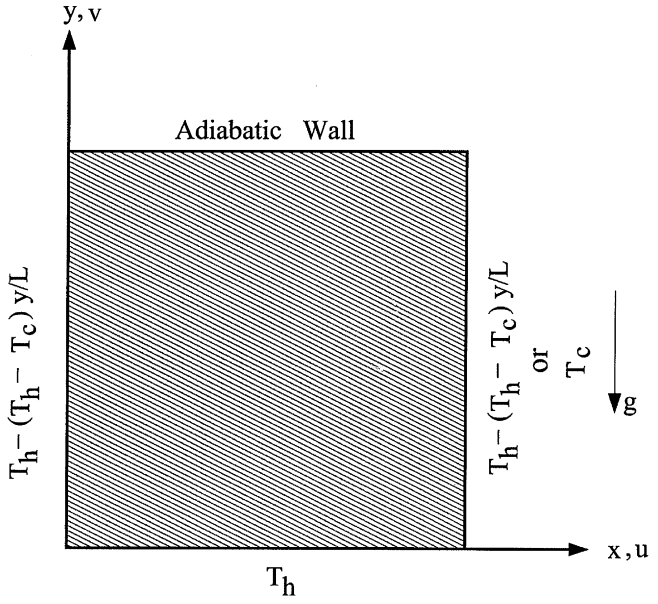

Fig. 1. Schematic diagram of the physical system.

corresponds to computational singularity. In particular, the singularity at the corner node of the bottom wall needs special mention. The grid size dependent effect of the temperature discontinuity at the corner points upon the local Nusselt numbers tend to increase as the mesh spacing at the corner is reduced. The difficulties are overcome by assuming the average temperature of the adjacent walls at the corner node and in the adjacent grid nodes at the respective wall temperatures.

In the current investigation, Gaussian quadrature based finite element method provides the smooth solutions at the interior domain including the corner regions as evaluation of residual depends on interior Gauss points and thus the effect of corner point is less pronounced in the final solution. The present finite element approach offers special advantage on evaluation of local Nusselt number at the bottom and side walls as the element basis functions are used to evaluate the heat flux.

4. Results and discussion

4.1. Effects of Rayleigh number

4.1.1. Case I: Linearly heated side walls

Figs. 2–7 illustrate the stream function and isotherm contours for various values of $Ra = 10^3$–10^5 and $Pr = 0.7$–10 with uniformly heated bottom wall and linearly heated side walls where the top wall is well insulated. As expected due to the linearly heated vertical walls and the uniformly heated bottom wall, fluids rise up from the middle portion of the bottom wall and flow down along two vertical walls forming two symmetric rolls with clockwise and anti-clockwise rotations inside the cavity. At $Ra = 10^3$, the magnitudes of stream functions are considerably lower and the heat transfer is due to purely conduction. During conduction dominant heat transfer, the temperature $\theta \leqslant 0.3$ occur symmetrically near the side walls of the enclosure. The other temperature contours with $\theta \geqslant 0.4$ are smooth curves which span the entire enclosure and they are generally symmetric with respect to the vertical symmetric line. The temperature contours as indicated in Fig. 2 remains invariant upto $Ra < 10^4$.

At $Ra = 10^4$, the circulation near the central regimes are stronger and consequently, the temperature contour with $\theta = 0.5$ starts getting shifted towards the side wall and break into two symmetric contour lines (see Fig. 3). The presence of significant convection is also exhibited in Fig. 4 at $Ra = 5 \times 10^4$ where temperature contour for $\theta = 0.6$ starts getting deformed and pushed towards the top plate. In addition, it may be noted that the secondary circulations appear at the bottom corners for $Ra = 5 \times 10^4$ due to convection as the lower half of the vertical walls are hot and the hot fluids move towards the center of the cavity. Consequently, at $Ra = 7 \times 10^4$ the stronger

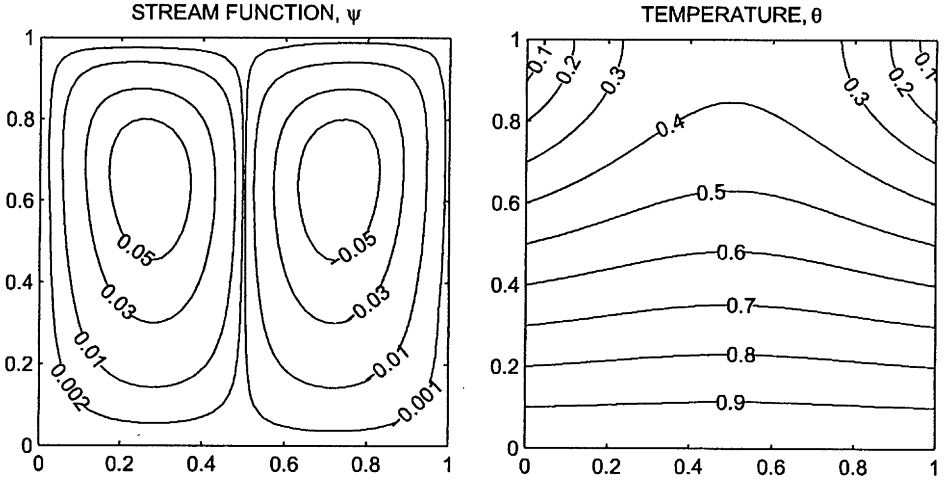

Fig. 2. Contour plots for linearly heated vertical walls $\theta(0, Y) = \theta(1, Y) = 1 - Y$, with $Pr = 0.7$ and $Ra = 10^3$. Clockwise and anti-clockwise flows are shown via negative and positive signs of stream functions, respectively.

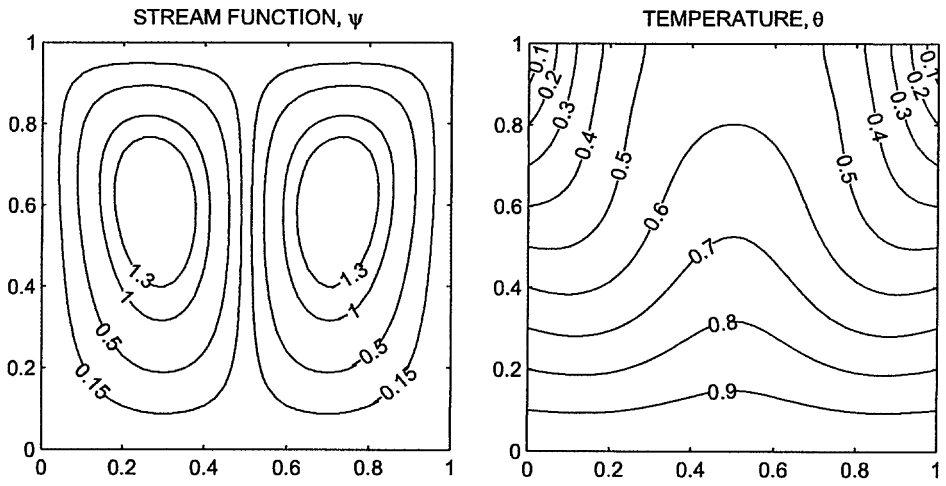

Fig. 3. Contour plots for linearly heated vertical walls $\theta(0, Y) = \theta(1, Y) = 1 - Y$, with $Pr = 0.7$ and $Ra = 10^4$. Clockwise and anti-clockwise flows are shown via negative and positive signs of stream functions, respectively.

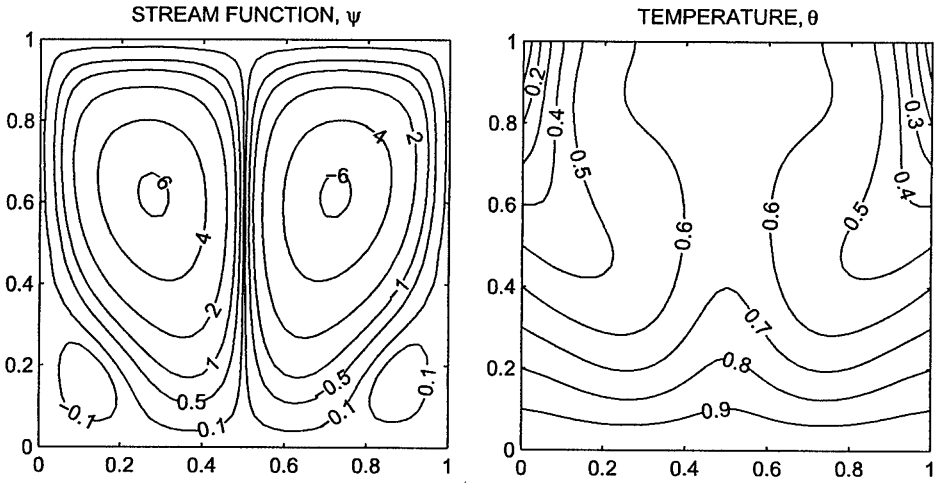

Fig. 4. Contour plots for linearly heated vertical walls $\theta(0, Y) = \theta(1, Y) = 1 - Y$, with $Pr = 0.7$ and $Ra = 5 \times 10^4$. Clockwise and anti-clockwise flows are shown via negative and positive signs of stream functions, respectively.

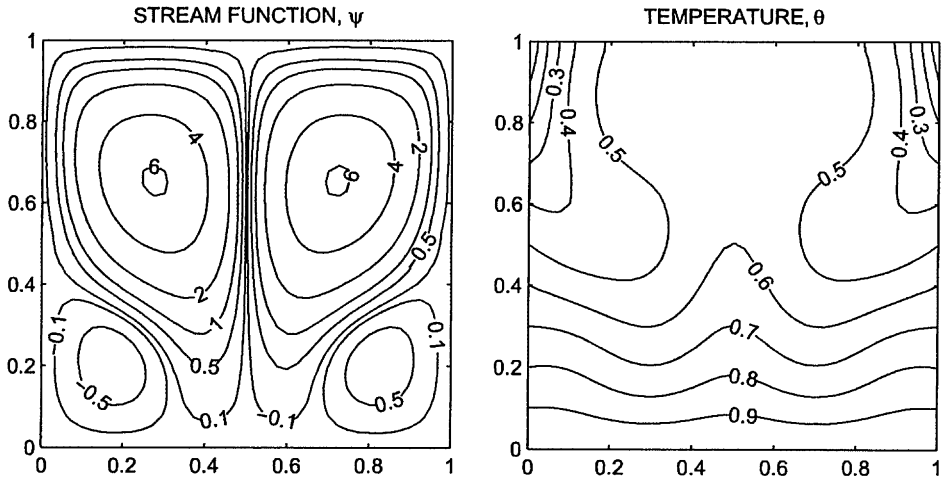

Fig. 5. Contour plots for linearly heated vertical walls $\theta(0, Y) = \theta(1, Y) = 1 - Y$, with $Pr = 0.7$ and $Ra = 7 \times 10^4$. Clockwise and anti-clockwise flows are shown via negative and positive signs of stream functions, respectively.

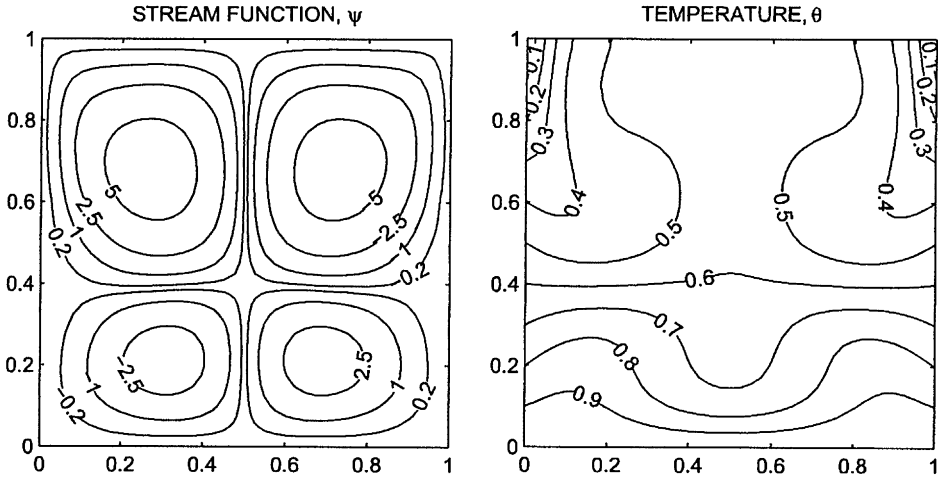

Fig. 6. Contour plots for linearly heated vertical walls $\theta(0, Y) = \theta(1, Y) = 1 - Y$, with $Pr = 0.7$ and $Ra = 10^5$. Clockwise and anti-clockwise flows are shown via negative and positive signs of stream functions, respectively.

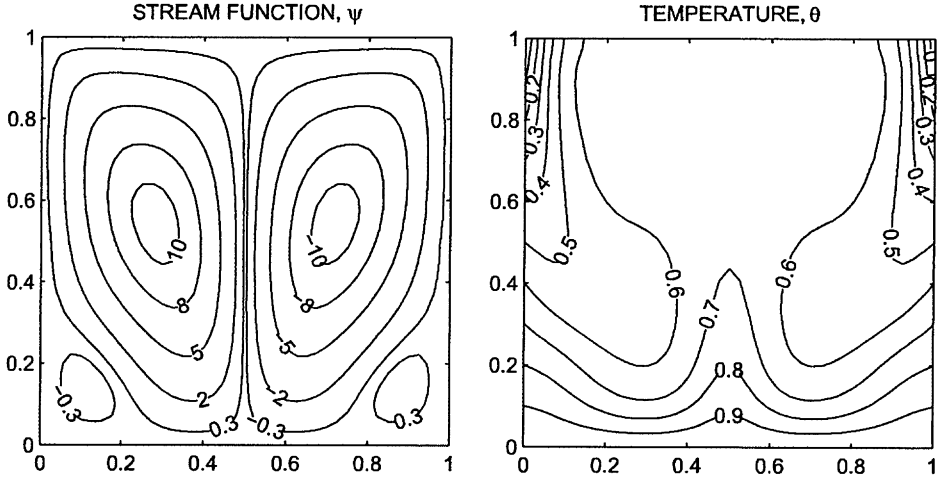

Fig. 7. Contour plots for linearly heated vertical walls $\theta(0, Y) = \theta(1, Y) = 1 - Y$, with $Pr = 10$ and $Ra = 10^5$. Clockwise and anti-clockwise flows are shown via negative and positive signs of stream functions, respectively.

secondary circulations enhance the mixing process which result in the rejoining of temperature contour $\theta = 0.6$ (Fig. 5). Further, at $Ra = 10^5$, the primary circulation pushed towards the upper part of the cavity and due to enhanced convection from the linear hot vertical wall, the isotherm lines with greater values $\theta > 0.5$ covers almost 70% of the cavity (Fig. 7). It is interesting to observe that due to two pairs of symmetric circulations, 'hot' and 'cold' fluid regimes appear distinctly across the temperature contour $\theta = 0.6$. In contrast, at $Ra = 10^5$ for $Pr = 10$, the strength of secondary circulations appearing at corners of bottom wall is less as compared for $Pr = 0.7$ case due to the viscus force dominating the buoyancy force for $Pr = 10$ (see Fig. 7). As the strength of the primary circulation increases for $Pr = 10$ case, the isotherm lines with temperature contours $\theta > 0.5$ covers approximately 90% of cavity. The significant effect of convective heat transfer will be illustrated later via average Nusselt number vs Rayleigh number plot.

4.1.2. Case II: Linearly heated left wall with cooled right wall

Figs. 8–11 illustrate the stream function and isotherm contours for various values of $Ra = 10^3$–10^5 and $Pr =$ 0.7–10 with uniformly heated bottom wall, cooled right wall and the left wall is linearly heated. As expected due to linearly heated left wall, fluids rise up along the side of left wall and flow down along the cooled right wall forming a roll with clockwise rotation inside the cavity. As Ra increase from 10^3 to 10^5, the value of stream function increases i.e., the flow rate increases. At the left corner of the top wall, secondary circulation formed due to convection, and the hot fluids move towards the left corner of the cavity. Fig. 8 shows that the isotherm lines change its

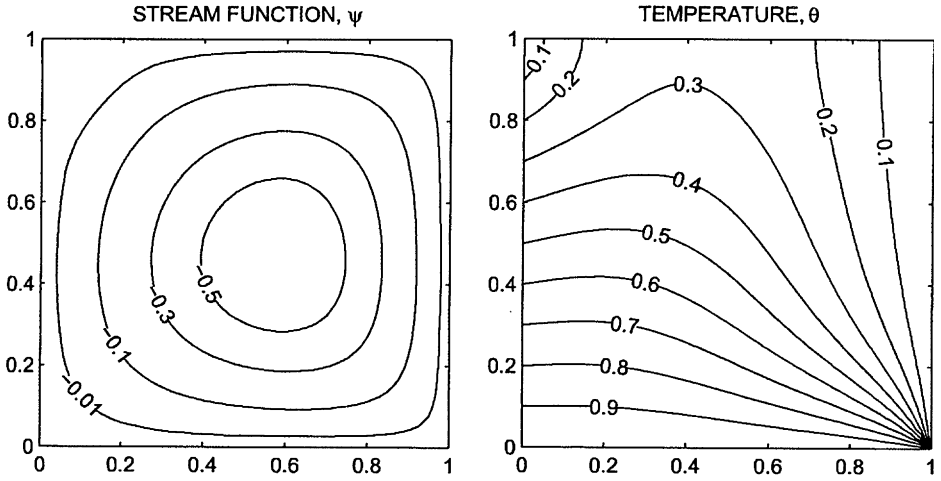

Fig. 8. Contour plots for linearly heated left vertical wall, $\theta(0, Y) = 1 - Y$ and cooled right vertical wall, $\theta(1, Y) = 0$, with $Pr = 0.7$ and $Ra = 10^3$. Clockwise and anti-clockwise flows are shown via negative and positive signs of stream functions, respectively.

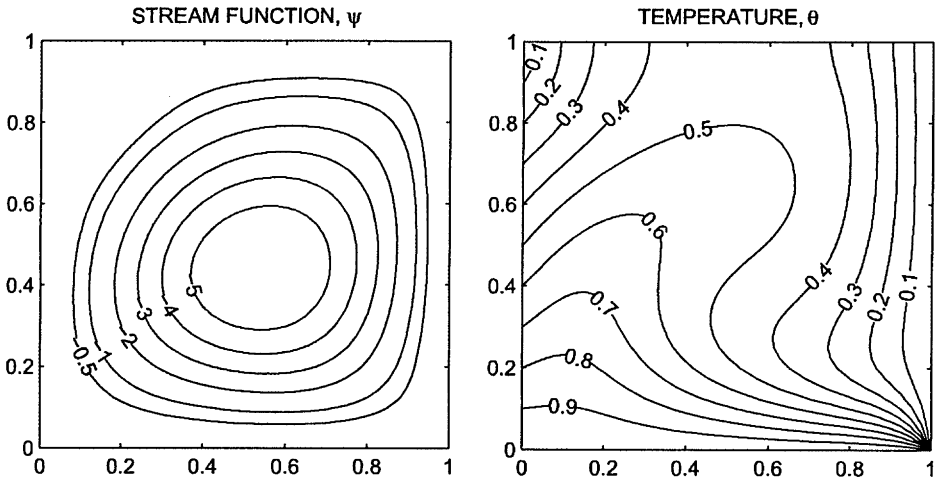

Fig. 9. Contour plots for linearly heated left vertical wall, $\theta(0, Y) = 1 - Y$ and cooled right vertical wall, $\theta(1, Y) = 0$, with $Pr = 0.7$ and $Ra = 10^4$. Clockwise and anti-clockwise flows are shown via negative and positive signs of stream functions, respectively.

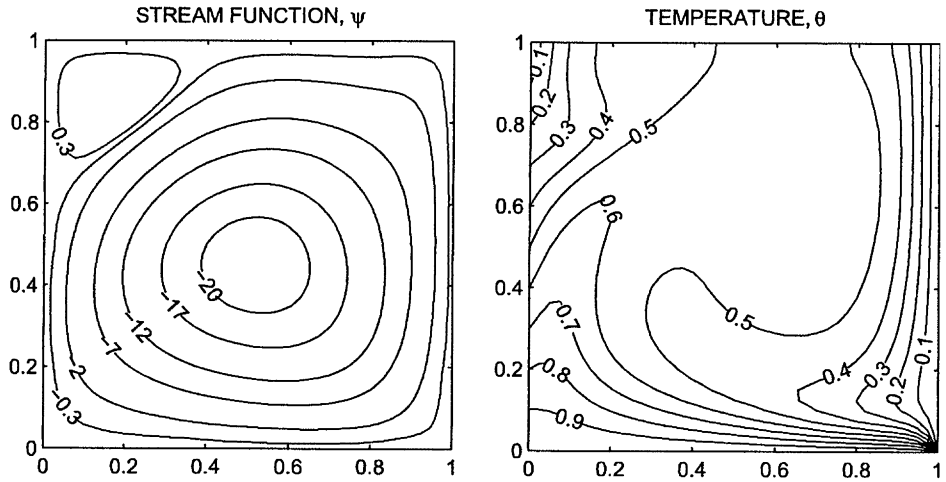

Fig. 10. Contour plots for linearly heated left vertical wall, $\theta(0, Y) = 1 - Y$ and cooled right vertical wall, $\theta(1, Y) = 0$, with $Pr = 0.7$ and $Ra = 10^5$. Clockwise and anti-clockwise flows are shown via negative and positive signs of stream functions, respectively.

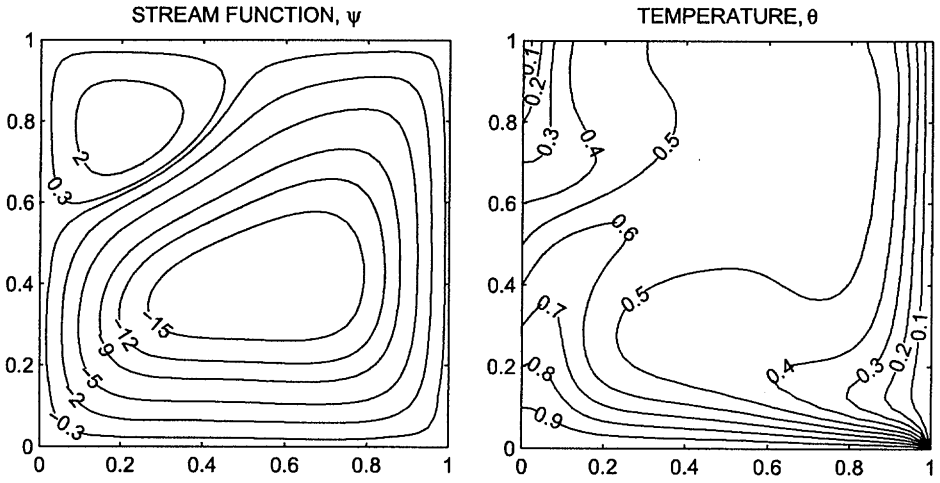

Fig. 11. Contour plots for linearly heated left vertical wall, $\theta(0, Y) = 1 - Y$ and cooled right vertical wall, $\theta(1, Y) = 0$, with $Pr = 10$ and $Ra = 10^5$. Clockwise and anti-clockwise flows are shown via negative and positive signs of stream functions, respectively.

value smoothly from hot vertical wall to cold vertical wall for $Ra = 10^3$.

At $Ra = 10^4$ the circulations are stronger and consequently, the temperature contour with $\theta = 0.5$ pushed towards the right corner of top wall (see Fig. 9). At $Ra = 10^5$ in Figs. 10 and 11 due to enhanced convection from the hot left wall to the cold right wall, the isotherm lines with greater values $\theta > 0.5$ covers around 50% of the cavity for $Pr = 0.7$ and $Pr = 10$. In addition for $Pr = 10$, the strength of secondary circulation increases.

4.2. Heat transfer rates: local and average Nusselt numbers

4.2.1. Case I: Linearly heated side walls

Fig. 12(a) and (b) display the effects of Ra and Pr on the local Nusselt numbers at the bottom and side walls (Nu_b, Nu_s) for linearly heated side walls. At the edges of the bottom wall, the heat transfer rate Nu_b, is 1 due to the linearly heated side walls (see Fig. 12(a)). For $Ra = 10^4$, the heat transfer rate is sinusoidal type with its minimum value at the center of the bottom wall due to the higher values of stream function (i.e., flow rate) with two symmetric circulations about the vertical symmetric line at the center of the bottom wall. Similar situation of sinusoidal heat transfer rate prevails at $Ra = 10^5$ and $Pr = 10$. In contrast, for $Ra = 10^5$ and $Pr = 0.7$, the heat transfer rate is maximum at center of the bottom wall due to the presence of strong secondary circulations leading to a high temperature gradient at the center of the bottom wall.

In Fig. 12(b), the heat transfer rate at the bottom-edge of side wall is zero due to uniformly heated bottom wall and the heat transfer rate is maximum at the top-edge of side wall due to insulated top wall. For $Ra = 10^3$, $Pr = 0.7$, due to weak circulations, the heat transfer rate is almost zero upto $Y = 0.7$ and $Nu_s = 3$ at $Y = 1$ whereas at $Ra = 10^4$, the heat transfer rate $Nu_s = 4$ at $Y = 1$ due to stronger circulations. For $Ra = 10^5$, due to the presence of a pair of symmetric secondary circulated cells with clockwise and anti-clockwise rotations, the heat transfer rate is oscillatory in nature in the lower half of the side walls and the increasing trend of heat transfer rate is observed in the upper half of the side walls with $Nu_s = 6$ and $Nu_s = 8$ at $Y = 1$ corresponding to $Pr = 0.7$ and $Pr = 10$, respectively.

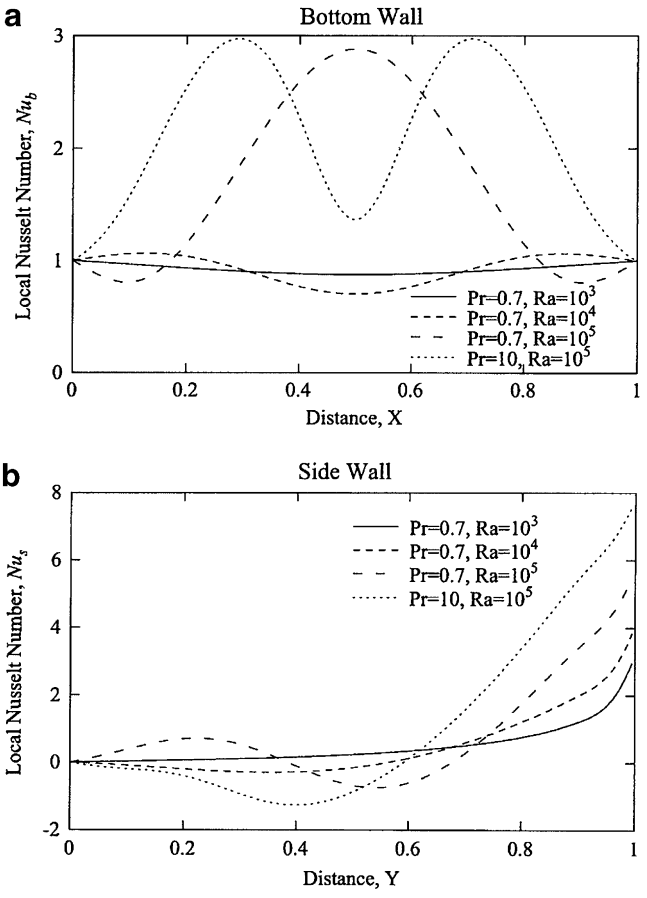

Fig. 12. Variation of local Nusselt number with distance at (a) bottom wall and (b) side wall for linearly heated side walls.

The overall effects upon the heat transfer rates are displayed for linearly heated side walls in Fig. 14(a) and (b),

where the distributions of the average Nusselt number of bottom wall and side walls, respectively, are plotted vs the Rayleigh number. It is observed that the average Nusselt number is almost constant upto $Ra = 10^4$ due to dominant heat conduction mode and smoothly increases as Rayleigh number increases further. It is interesting to note that the smoothness breaks at $Ra = 7 \times 10^4$ and $Pr = 0.7$ for both bottom and side walls as the oppositely rotated secondary cells becomes prominent. The smoothly increasing trend of average Nusselt numbers is observed for $Pr = 10$ due to insignificant secondary cells.

4.2.2. Case II: Linearly heated left wall with cooled right wall

Fig. 13(a) and (b) display the effects of Ra and Pr on local Nusselt numbers at the bottom and side walls (Nu_b, Nu_l, Nu_r) for linearly heated left wall and cooled right wall. The heat transfer rate Nu_b is 0 at the left-edge of the bottom wall due to the linearly heated left wall and it is maximum at the right-edge of the bottom wall due to the cooled right wall (see Fig. 13(a)). As Ra increases from 10^3 to 10^5, the heat transfer rate increases from the left-edge to the right-edge of the bottom wall.

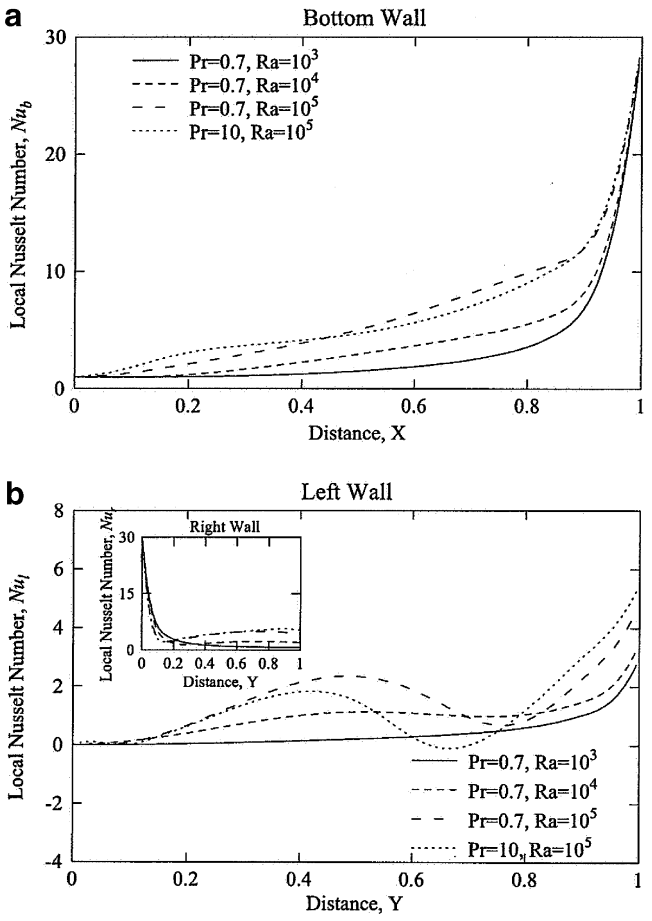

Fig. 13. Variation of local Nusselt number with distance at (a) bottom wall and (b) left and right walls for linearly heated left wall and cooled right wall.

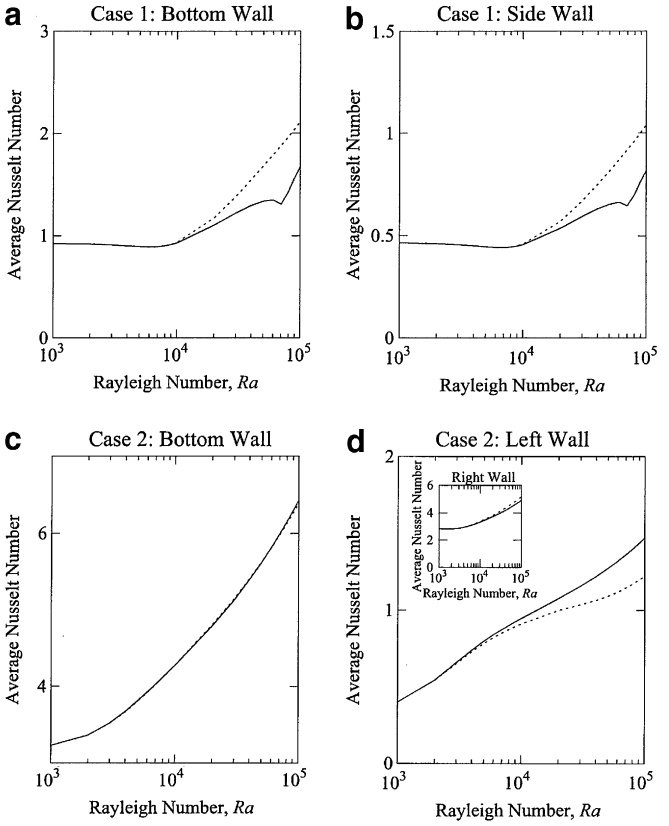

Fig. 14. Variation of average Nusselt number with Rayleigh number for linearly heated side walls [(a) and (b)] and linearly heated left wall and cooled right wall [(c) and (d)] with $Pr = 0.7$ (—) and $Pr = 10$ (---). The inset of (d) shows plot of average Nusselt number vs Rayleigh number for right wall.

In Fig. 13(b), the heat transfer rate (Nu_l) at the bottom edge of the left wall is zero due to the uniformly heated bottom wall and linearly heated left wall and its magnitude increases from the bottom edge to the top edge of the left wall. At $Ra = 10^5$, local Nusselt number (Nu_l) exhibits oscillatory behavior due to the presence of secondary circulation near the top edge of the left wall. The inset plot shows the local Nusselt number (Nu_r) distribution for the right wall. For all values of Ra and Pr, it is observed that Nu_r is maximum at the bottom edge and decreases towards the top edge.

The overall effects of Ra and Pr on the average Nusselt numbers at the bottom and side walls are displayed in Fig. 14(c) and (d). It is observed that the average Nusselt numbers smoothly increase as Rayleigh number increases except for $Pr = 10$ at the left wall due to the presence of strong secondary cell. In contrast, the average Nusselt numbers at side walls were found to be increased with Prandtl number as discussed for case I.

5. Conclusions

The influence of linearly heated vertical wall(s) with uniformly heated bottom wall on flow and heat transfer characteristics due to natural convection within a square

enclosure has been studied in the present investigation. The penalty finite element method helps to obtain smooth solutions in terms of stream function and isotherm contours for a range of Pr and Ra. In case of linearly heated side walls, for large values of $Ra \geqslant 7 \times 10^4$, the presence of a pair of symmetric strong secondary circulations enhances the local mixing process in the lower half of the cavity and the local Nusselt numbers (Nu_s) are found to be oscillating in nature at the lower half of the side walls with an usual increasing trend in the upper half of the side walls due to the insulated top wall. Moreover, the average Nusselt number is almost constant upto $Ra = 10^4$ due to dominant heat conduction mode, and smoothly increases as Rayleigh number increases further but the smoothness breaks at $Ra = 7 \times 10^4$ for $Pr = 0.7$ for both bottom and side walls as the oppositely rotating side walls become prominent. In contrast for the case of linearly heated left wall and cooled right wall, at $Ra = 10^5$, local Nusselt number at the left wall exhibits oscillatory behavior due to the presence of secondary circulation near the top edge of the left wall. Further, the average Nusselt numbers smoothly increase as Rayleigh number increases with an exception for $Pr = 10$ at the left wall due to the presence of strong secondary cell near the top edge of the left wall.

References

[1] S. Ostrach, Natural convection in enclosures, Advances in Heat Transfer, vol. VII, Academic Press, New York, 1972, pp. 161–227.

[2] S. Ostrach, Low-gravity fluid flows, Annu. Rev. Fluid Mech. 14 (1982) 313–345.

[3] S. Ostrach, Natural convection in enclosures, ASME Trans. J. Heat Transfer 110 (1988) 1175–1190.

[4] B. Gebhart, Buoyancy induced fluid motions characteristics of the applications in technology, The 1978 Freeman Scholar Lecture, ASME Trans. J. Fluids Eng. 101 (1979) 5–28.

[5] C.J. Hoogendoorn, Natural convection in enclosures, in: Proc. Eight Int. Heat Transfer Conf., vol. I, Hemisphere Publishing Corp., San Francisco, 1986, pp. 111–120.

[6] T. Fusegi, J.M. Hyun, K. Kuwahara, Natural convection in a differentially heated square cavity with internal heat generation, Numer. Heat Transfer Part A 21 (1992) 215–229.

[7] J.L. Lage, A. Bejan, The *Ra–Pr* domain of laminar natural convection in a enclosure heated from the side, Numer. Heat Transfer Part A 19 (1991) 21–41.

[8] J.L. Lage, A. Bejan, The resonance of natural convection in a enclosure heated periodically from the side, Int. J. Heat Mass Transfer 36 (1993) 2027–2038.

[9] C. Xia, J.Y. Murthy, Buoyancy-driven flow transitions in deep cavities heated from below, ASME Trans. J. Heat Transfer 124 (2002) 650–659.

[10] M. November, M.W. Nansteel, Natural convection in rectangular enclosures from below and cooled along one side, Int. J. Heat Mass Transfer 30 (1987) 2433–2440.

[11] A. Valencia, R.L. Frederick, Heat transfer in a square cavities with partially active vertically walls, Int. J. Heat Mass Transfer 32 (1989) 1567–1574.

[12] M.M. Ganzarolli, L.F. Milanez, Natural convection in a rectangular enclosures heated from below and symmetrically cooled from the sides, Int. J. Heat Mass Transfer 38 (1995) 1063–1073.

[13] M. Corcione, Effects of the thermal boundary conditions at the sidewalls upon natural convection in rectangular enclosures heated from below and cooled from above, Int. J. Heat Mass Transfer 42 (2003) 199–208.

[14] I.E. Sarris, I. Lekakis, N.S. Vlachos, Natural convection in a 2D enclosure with sinusoidal upper wall temperature, Numer. Heat Transfer Part A 42 (2002) 513–530.

[15] J.N. Reddy, An Introduction to Finite Element Method, McGraw-Hill, New York, 1993.

[16] S. Roy, T. Basak, Finite element analysis of natural convection flows in a square cavity with nonuniformly heated wall(s), Int. J. Eng. Sci. 43 (2005) 668–680.

[17] G.K. Batchelor, An Introduction to Fluid Dynamics, Cambridge University Press, 1993.

[18] G.D. Mallinson, G.D. Vahl Davis, Three-dimensional natural convection in a box: a numerical study, J. Fluid Mech. 83 (1977) 1–31.